

Local energy-based multimodal medical image fusion in curvelet domain

Richa Srivastava¹, Om Prakash², Ashish Khare¹✉

¹Department of Electronics and Communication, University of Allahabad, Allahabad, India

²School of Information and Communication, Gwangju Institute of Science and Technology (GIST), Gwangju, South Korea

✉ E-mail: khare@allduniv.ac.in

Abstract: Various multimodal medical images like computed tomography (CT), magnetic resonance imaging (MRI), positron emission tomography, single photon emission CT and structural MRI have different characteristics and carry different types of complementary anatomical and functional information. Therefore, fusion of multimodal images is required, in order to achieve good spatial resolution images carrying both anatomical and functional information. In this work, the authors have proposed a fusion technique based on curvelet transform. Curvelet transform is a multiscale, multidirectional transform having anisotropic property and is very efficient in capturing edge points in images. Edges in an image are the important information carrying points used to show better visual structure of the image. They use local energy-based fusion rule which is more effective than single pixel-based fusion rules. Comparison of the proposed method with other existing spatial and wavelet transform based methods, in terms of visual and quantitative measures show the effectiveness of the proposed method. For quantitative analysis of the method, they used five fusion metrics as entropy, standard deviation, sharpness and average gradient.

1 Introduction

Medical image fusion [1, 2] is an interesting and rapidly growing research field in the area of medical imaging. Due to the evolution of various medical image sensors, different multimodal medical images are available [3] for clinical analysis and diagnosis purpose. These images are either anatomical or functional images. The anatomical images provide information about the structure of a particular part of the human body. For example, the computed tomography (CT) images carry the dense structure of the body parts like bones, muscles, organs and so on, whereas magnetic resonance imaging (MRI) gives excellent delineation of soft tissue structures of the body. On the other hand, functional images like positron emission tomography (PET) and single position emission CT (SPECT) provide functional information or changes in the normal shape or size of organs. CT and MRI images are of good spatial quality, whereas PET and SPECT images are of low spatial quality [3, 4]. These examples show that, to obtain complete and accurate information with good spatial resolution, we need to combine these multimodal images using an image processing technique.

Image fusion [5] is a process that integrates information from two or more images of different modality and renders a single composite image, containing all the relevant information of source images without creating any artefact or noise. The fused image describes the scene better than any individual source image. The basic objective of fusion is to produce a complementary image carrying enhanced visual image content to make it more informative for analysis, which is suitable for different medical or other image processing applications.

A series of image fusion methods [6–8] has been developed in the recent past. The existing fusion methods have been categorised, on the basis of level where fusion is performed. There are three basic levels of fusion – pixel level fusion [6], feature level fusion [7] and decision level fusion [8]. Pixel level fusion is the lowest level of fusion, in which, fusion is performed directly on the pixels of source images. Yang and Li [6] have given an overview of pixel level fusion algorithms, their strengths and shortcomings. In feature level fusion, unlike pixel-by-pixel selection, area-based selection is used [1, 7]. In this fusion method, different objects are extracted from the source images and then, they are fused depending on their features. It performs better than pixel level

fusion methods and is least affected by noise or other artefacts. However, in multimodal image fusion, the feature spaces are generally incompatible, which create problems in the fusion process. The third and the highest level of fusion is a decision level fusion [8]. This type of fusion uses statistics, voting, fuzzy logic or heuristics for decision making, before performing fusion. One of the examples of decision level fusion is a biometric verification. As compared to feature and decision level fusion, the image fused by pixel level fusion methods preserve information content of the original images more accurately. Pixel level fusion methods are the simplest and efficient over other types of fusion methods [1, 5].

There are several researches that use pixel level fusion methods either in spatial domain [9] or in wavelet domain [10–13]. In spatial domain methods, fusion is performed directly on the pixel values of images. Averaging, weighted averaging, Brovey transform, principal component analysis (PCA), are few examples of spatial domain methods. The fused images obtained by applying spatial domain based methods are generally of reduced contrast and contain low information content [14]. To overcome these problems, other pixel level fusion methods based on multiscale transforms have been developed. The basic concept of multiscale transforms based methods is, first, to transform the source images into its frequency parts and then, apply fusion rules to combine the image information in each subpart separately. The fused image is then, reconstructed by applying the inverse transform. Laplacian pyramid (LP) [10], ratio-of-low-pass pyramid, morphological pyramid and wavelet transform [11] are popular multiscale fusion methods. Pyramid transform [14] is used by many researchers and has given satisfactory performance, but, it suffers from blocking effect, redundancy and lack of directional information [11] problems. On the other hand, wavelet based methods provide comparatively better results. Localisation and multi-directional features of wavelet transform make it superior to pyramid transform and have given excellent results in case of one dimensional signals. However, in two-dimensional cases, its performance is not satisfactory. Wavelets cannot capture the discontinuities along the curves and edges effectively, due to its limited number of directions. Hence, the images fused by wavelet transform are of poor spatial quality [12, 13].

Recently, curvelet transform [15–17] has been introduced to reduce the limitations of wavelet transform. Curvelet transform is highly directional and anisotropic in nature. It has needle-shaped

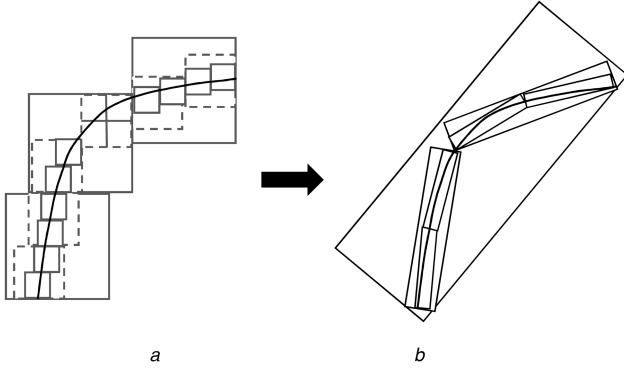


Fig. 1 Example of curve representation using wavelet and curvelet in non-linear approximation
a Wavelet representation
b Curvelet representation
(Each cell shows a coefficient)

basis elements that can efficiently capture the curves and edges of the real images. Hence, it is more suitable for many image processing applications [18–20] especially for image fusion. After the development of curvelet transform, some image fusion methods have been developed using curvelet transform. Nehcini *et al.* [12] have given curvelet transform-based image fusion for remote sensing images. Li and Yang [13] have proposed a multifocus image fusion method in which they have combined curvelet transform with wavelet transform to avail benefits of both the transforms. Another region-based image fusion method in curvelet domain is proposed by Mahyari and Yazdi [21]. All of these methods have used complex algorithm for fusion. In this paper, we have proposed a simple and efficient fusion method based on local energy in curvelet domain.

In image fusion, selection of fusion rule is very crucial, because the fusion results profoundly depend on it. An improper selection of fusion rule may yield suboptimal results. In the proposed work, we have used the local energy-based fusion rule. Here, selection of curvelet coefficient at a particular location depends on curvelet coefficients of that location and its neighbourhood locations. Local energy-based fusion rule is more reliable than single pixel-based fusion rules, such as absolute maximum selection fusion rule [22], edge preserving fusion rule [23], because here, the decision is based on neighbourhood elements as well. Therefore, the probability of selection of incorrect coefficient is much less than the single point-based fusion rules. For fusion process, we need to register images. The registration process is out of scope to this work and we assumed that pre-registered medical images are available for the fusion purpose.

The rest of the paper is organised as follows: Section 2 gives an overview of curvelet transform. Section 3 elaborates the proposed fusion method. Section 4 describes the image quality evaluation metrics used to assess the fusion performance. In Section 5, we have presented the fusion results of the proposed method and other methods used in comparison. Finally, concluding remarks of the proposed work are given in Section 6.

2 Curvelet transform

Donoho and Flesia [24] proposed a new powerful transform called ridgelet transform. Ridgelet transform is anisotropic in nature and can efficiently capture the global straight line singularities. However, in real images, global straight line is not so common. To handle this situation, the whole image is partitioned into small sub images. This partitioning is done in a manner so that the curves and edge lines appear just as a straight line. Ridgelet transform is then applied on each sub image. This block-based ridgelet transform is the basic concept of first generation curvelet transform [15, 16].

The theoretical idea of first generation curvelet is easy to understand, but, its implementation in discrete domain is difficult. Also, it is not quite popular because of its dependency on ridgelet transform whose geometry is very unclear. After one year, Candes *et al.* [17] came up with discrete version of curvelet transform,

which is based on frequency partition. This version of curvelet transform is efficient for representing curves and edges [15]. Unlike wavelet transform, curvelet transform is localised in scale, position and orientation [15, 16]. Due to these properties, curvelet transform can give efficient results for image fusion. The traditional wavelet is popular in image processing, but, its isotropic nature makes it inefficient in capturing line singularities. As shown in Fig. 1, it is clear that wavelet representation needs more coefficients than curvelet representation for representing the same curve. Hence, discrete curvelet transform is faster in capturing edges than wavelet and other transforms.

The discrete version of curvelet transform can be implemented in two ways. The first one is wrapping-based curvelet transform [17] and the second one is unequally-spaced fast Fourier transform (USFFT)-based curvelet transform [17]. These two implementations use different spatial grids for translation of curvelet at different scales and directions. In wrapping-based implementation, same translation grid is used for every angle within each quadrant. Therefore, it is easy to understand. On the other hand, in USFFT implementation, the grid is inclined according to the orientation of curvelet. It gives a more efficient implementation of discrete curvelet transform than wrapping-based implementation. Wrapping-based implementation has to perform 4/3 times more computations and requires more storage space than USFFT-based implementation [17]. Hence, for the above reasons we used USFFT-based implementation of curvelet transform in the implementation of our proposed method.

The basic structure of digital curvelet transform, based on USFFT implementation is divided into four steps.

- Subband decomposition:* An image I is divided into several decomposition levels with the help of low-pass filter P_0 and several band-pass filter banks, $\Delta_s, s \geq 0$. Image I is decomposed using à trous algorithm

$$I \rightarrow (P_0 I, \Delta_1 I, \Delta_2 I, \dots) \quad (1)$$

- Smooth partitioning:* Each subband is partitioned smoothly into ‘squares’ of proper scales

$$\Delta_s I \rightarrow (w_Q \Delta_s I)_{Q \in Q_s} \quad (2)$$

where w_Q is smooth window localised around dyadic squares

$$Q = \left[\frac{k_1}{2^s}, \frac{(k_1 + 1)}{2^s} \right] \times \left[\frac{k_2}{2^s}, \frac{(k_2 + 1)}{2^s} \right] \quad (3)$$

- Renormalisation:* The resulting dyadic squares are renormalised into unit scale of $[0, 1]^2$

$$g_Q = (T_Q)^{-1}(w_Q \Delta_s I), \quad Q \in Q_s \quad (4)$$

- Ridgelet analysis:* The normalised dyadic square is analysed by ridgelet system. It has basis elements p_λ that make an orthonormal basis for $L^2(\mathbb{R}^2)$:

$$\alpha_\mu = \langle g_Q, p_\lambda \rangle \quad (5)$$

3 Proposed method

Medical images are of different modalities and carry complementary information. For accurate and fast diagnosis, all these information must be extracted into a single image. In this work, we have proposed a curvelet transform-based image fusion method. There are many reasons for choosing curvelet transform. Curvelet transform is a non-separable, multiscale and multidirectional transform. Being anisotropic in nature, it has a better representation of edges than wavelet and other transforms, which is intrinsically beneficial for fusion. Needle-shaped basis elements of curvelet transform can efficiently capture the curves and edges. Hence, it is expected to give better fusion results.

The first step of the proposed method is to transform the source images into curvelet coefficient sets of different resolutions. These coefficient sets are then combined using local energy-based fusion

	$C(i-1, j-1)$	$C(i-1, j)$	$C(i-1, j+1)$	
	$C(i, j-1)$	$C(i, j)$	$C(i, j+1)$	
	$C(i+1, j-1)$	$C(i+1, j)$	$C(i+1, j+1)$	

Fig. 2 Illustration of local energy computation. $C(i, j)$, denotes curvelet coefficient at the (i, j) th spatial location

particular coefficient depends on that coefficient along with its neighbouring coefficients. The edges normally span over two or more pixels. Therefore, if a coefficient represents an edge then its neighbouring coefficients will also represent edge. Hence, selection of coefficient based on local energy is effective for capturing the edges. This fusion rule is also effective when images are corrupted by noise. Since, noise is generally isolated and therefore, the neighbouring coefficients corrupted with noise may have low absolute value. Hence, the noisy coefficients can easily be differentiated from the actual edge coefficients. Hence, noise cannot have much effect on the fused image if fusion is performed using local energy-based fusion rule.

Now, we elaborate the local energy-based fusion rule. If C is a matrix of transform coefficients. Taking a window of size 3×3 around a particular coefficient value, and local energy of centre pixel coefficient, can be calculated as the sum of squares of values of all the coefficients within the window. This window is moved around the image to calculate local energy of all other coefficients in the transformed image coefficients. In Fig. 2, we illustrated computation of local energy using neighbouring pixel coefficients.

The local energy at centre coefficient is defined as below:

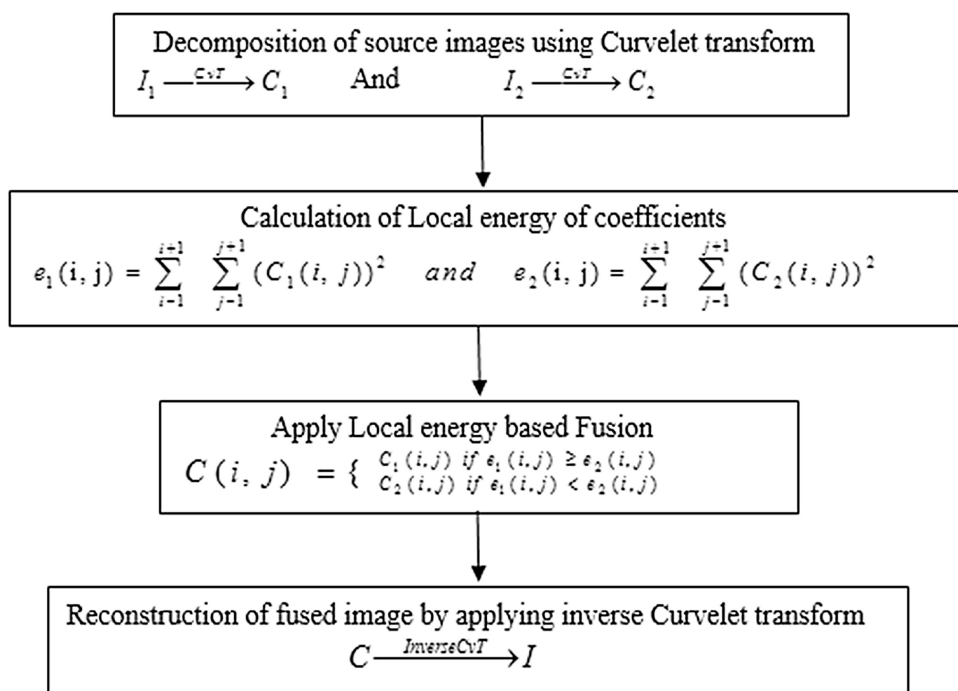


Fig. 3 Overall fusion procedure of the proposed method

rule. At last, the fused image is obtained by applying inverse curvelet transform on the combined coefficient sets. The multiresolution curvelet coefficients of different scales have different characteristics. The lower scales contain low frequency coefficients whereas the higher scales contain high frequency coefficients. The high frequency coefficients are more significant because they represent the salient features (edges, curves etc.) of an image. Therefore, our main focus is on the selection of high frequency coefficients, so that, it can preserve all the salient features of source images. The next step in the fusion process is the selection of suitable fusion rule. The fusion rule should be able to capture maximum relevant features of the source images. In the proposed algorithm, we have used local energy-based fusion rule. Local energy-based fusion rule [25, 26] is more effective and efficient than many other fusion rules, especially which are based on single coefficient (like absolute maximum and edge preserving fusion rule) [26–28]. In absolute maximum fusion rule, the absolute value of only single coefficient decides which coefficient is to be selected for the fused image. In the presence of noise, dependency on single coefficient may lead to inaccurate results, as transform coefficient corresponding to noise generally have higher absolute value. In local energy-based fusion rule, the selection of a

$$e_{i,j} = \sum_{i=1}^{i+1} \sum_{j=1}^{j+1} (c_{i,j})^2 \quad (6)$$

If local energy of centre coefficient is high, then centre coefficient and its surrounding coefficients are more likely to correspond an edge. Hence, we compare the value of local energy of curvelet coefficients, of source images, and select the coefficients with higher value of local energy. In this way, we select the transformed coefficients of the fused image. These coefficients are then, used to reconstruct the fused image by inverse curvelet transformation. In this fusion rule, probability of error is very small in comparison to other single coefficient-based fusion rules. The overall fusion procedure of the proposed method is depicted in Fig. 3.

4 Image quality assessment

The primary goal of image fusion is to improve the visual appearance, spectral and spatial qualities of an image. Hence, an effective fusion algorithm should improve an image in all these three aspects. The improvement related judgment is not an easy task because human eyes are not so perfect in observing very small differences in images. Hence, objective methods [29, 30] were

developed to evaluate the quality of images. These methods are of two types. The first type, in which a reference image is known and the fused image is compared with the reference image and the second type, in which, the reference image is not available. We have used the second type of objective methods because; in most of the fusion applications the reference image is not known. In this work, we have considered following five quantitative evaluation metrics.

4.1 Entropy

Entropy is the measure of information content of an image. It is calculated with the histogram counts

$$\text{Entropy} = \sum_{i=0}^{L-1} p_i \times \log_2(p_i) \quad (7)$$

where L is the number of grey level. p_i is the ratio of number of pixels having grey level i to the total number of pixels, i.e.

$$p_i = \frac{\text{Number of pixels with grey level } i}{\text{Total number of pixels}} \quad (8)$$

Higher the entropy value better is the image quality.

4.2 Standard deviation

Standard deviation represents the variation from the average value. It reflects the contrast of image. Higher the value of standard deviation, higher is the contrast of image. Hence, a good quality image should have a large value of standard deviation. Standard deviation is defined as

$$\sigma = \sqrt{\frac{1}{M \times N} \sum_{i=1}^M \sum_{j=1}^N (I(i, j) - \mu)^2} \quad (9)$$

where $I(i, j)$ is the intensity of image at positions (i, j) and μ is the mean intensity of the image. $M \times N$ is the size of image.

4.3 Edge strength (Q_{AB}^F)

Edge strength (Q_{AB}^F) metric represents the edge information associated with the fused image and visually supported by human visual system. To define Q_{AB}^F , consider two input images A and B , and fused image F . Edge strength $g(n, m)$ and orientation $\alpha(n, m)$ for each image pixel is computed by Sobel edge operator. For input image A , it is given by

$$g_A(n, m) = \sqrt{s_A^x(n, m)^2 + s_A^y(n, m)^2} \quad (10)$$

$$\alpha_A(n, m) = \tan^{-1}\left(\frac{s_A^y(n, m)}{s_A^x(n, m)}\right) \quad (11)$$

where $s_A^x(n, m)$ and $s_A^y(n, m)$ are the outputs of the horizontal and vertical Sobel templates centred on pixel $p_A(n, m)$ and convolution being performed with the corresponding pixels of image A . The relative edge strength $G^{AF}(n, m)$ and orientation preservation values $A^{AF}(n, m)$ of an input image A with respect to fused image F are formed as

$$G^{AF}(n, m) = \begin{cases} g_F(n, m) / g_A(n, m) & \text{if } g_A(n, m) > g_F(n, m) \\ g_A(n, m) / g_F(n, m) & \text{otherwise} \end{cases} \quad (12)$$

and

$$A^{AF}(n, m) = \frac{|\alpha_A(n, m) - \alpha_F(n, +)| - \pi/2|}{\pi/2} \quad (13)$$

Perceptual loss of information in the fused image for each pixel value of input image A is computed as below:

$$Q_g^{AF}(x, y) = \frac{\Gamma_g}{1 + e^{k_g(G^{AF}(n, m) - \sigma_g)}} \quad (14)$$

$$Q_\alpha^{AF}(n, m) = \frac{\Gamma_\alpha}{1 + e^{k_\alpha(A^{AF}(n, m) - \sigma_\alpha)}} \quad (15)$$

Here constants Γ_g , k_g , σ_g and Γ_α , k_α , σ_α determine the exact shape of the sigmoid functions used to form the edge strength and orientation preservation values. Edge information preservation values are defined as follows:

$$Q^{AF}(n, m) = Q_g^{AF}(n, m)Q_\alpha^{AF}(n, m) \quad (16)$$

with $0 \leq Q^{AF}(n, m) \leq 1$. Value zero (0) denotes the complete loss of edge information in fused image and value one (1) indicates fusion with no loss of edge information.

A normalised weighted performance metric Q_{AB}^F is obtained by having edge preservation values for both input images A and B i.e. $Q^{AF}(n, m)$ and $Q^{BF}(n, m)$ is given by

$$Q_{AB}^F = \frac{\sum_{n=1}^N \sum_{m=1}^M Q^{AF}(n, m)w^A(n, m) + Q^{BF}(n, m)w^B(n, m)}{\sum_{i=1}^N \sum_{j=1}^M (w^A(i, j) + w^B(i, j))} \quad (17)$$

where $w^A(n, m)$ and $w^B(n, m)$ are weights for edge preservation values $Q^{AF}(n, m)$ and $Q^{BF}(n, m)$, respectively.

Q_{AB}^F is a unit less quantity, whose value lies between zero (0) and one (1). A higher value of metric Q_{AB}^F implies fused image with better edge information and hence rich in visual content.

4.4 Sharpness

Sharpness of an image represents the small details of the image. Since, the small details make the quality of image better, hence better image should have high value of sharpness. Sharpness is defined as

$$SP = \frac{1}{MN} \sum_{i,j} \sqrt{\frac{(I(i, j) - I(i, j-1))^2 + (I(i, j) - I(i-1, j))^2}{2}} \quad (18)$$

where $I(i, j)$ is the intensity of image of size $M \times N$ at locations (i, j) .

4.5 Average gradient

It reflects the clarity of an image. Average gradient is defined as below:

$$AG = \frac{1}{(M-1)(N-1)} \sum_{i=1}^{M-1} \sum_{j=1}^{N-1} \sqrt{\frac{1}{2} \left(\left(\frac{\partial I(i, j)}{\partial i} \right)^2 + \left(\frac{\partial I(i, j)}{\partial j} \right)^2 \right)} \quad (19)$$

where I is the source image of size $M \times N$. Better quality image should have higher value of average gradient.

5 Results and discussion

In this section, we present experimental settings in Section 5.1 and experimental results of the proposed method in Section 5.2. We have compared our results with several spatial domain (PCA [9] and sharp fusion [31]) and transform domain (LP [14], stationary wavelet transform (SWT) [32] and discrete wavelet transform (DWT) [33], dual tree complex wavelet transform (DTCWT) [34], lifting wavelet transform (LWT) [35], multi-wavelet transform (MWT) [36], Daubechies complex wavelet transform (DCxWT) [22] and non-subsampled contourlet transform (NSCT) [25]) methods. The results of methods used in comparison have also

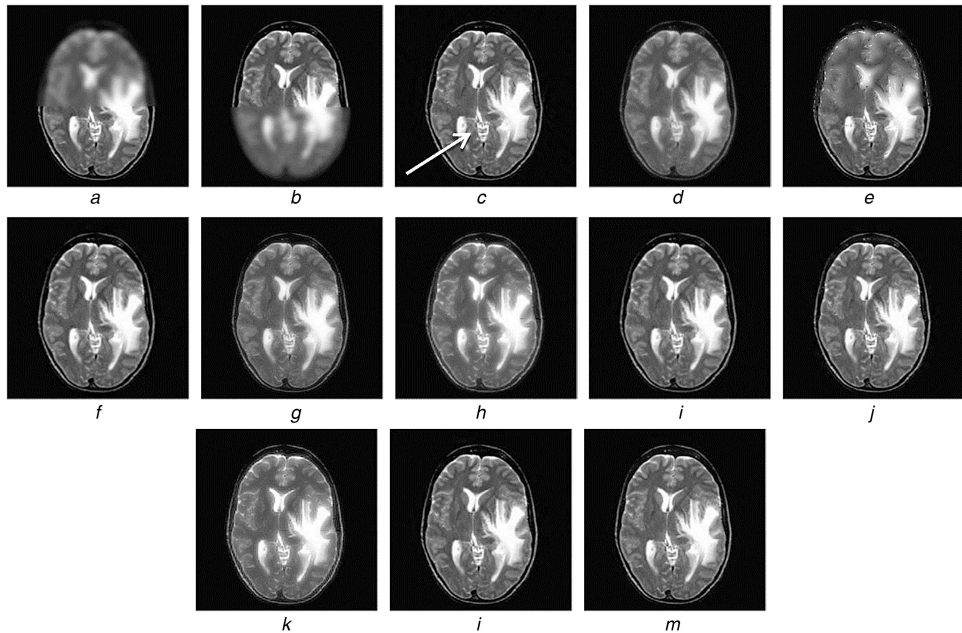


Fig. 4 Fusion results of first set of medical images. *a* and *b* are source images

a Blurred on upper half

b Blurred on lower half

c–m Fusion results of the proposed and other methods. Better visual structure can be easily observed at the region indicated by an arrow

been presented in Section 5.2. Finally, observations, analyses and discussions have been given in Section 5.3.

5.1 Experimental settings and dataset

The proposed method of image fusion has been tested on several pairs of medical images of different modalities. The experiments have been performed using Matlab 2011a on a PC having 1.9 GHz Core 2 duo processor and 2 GB memory. The fusion has been performed on images of the size 256×256 pixels. The first set of medical images contains two blurred images, one is blurred on the upper half and other is blurred on the lower half. Second and fourth sets of medical images contain a CT image and an MRI image. CT and MRI images capture information that are complementary to each other. The principle of CT is based on varying absorption of X-ray by different tissues and generates cross-sectional images. The MRI technique is based on the principle of nuclear-magnetic resonance. It generate images by an absorption-release pattern of energy. The CT images carry information of hard tissues like bones and muscles. On the other hand, the MRI images carry information of soft tissues. The third set of medical images contains a T1-weighted MRI image and an MRA image. The MRA image contains some abnormality in the form of white calcified structure, whereas the T1-weighted MRI is unable to detect these abnormalities. The other six sets of images contain T1-weighted MRI and T2-weighted MRI image pairs. The T1-weighted MRI image gives detail information about anatomical structures of the body, whereas the T2-weighted MRI image accurately differentiates between normal and abnormal tissues. Therefore, the dataset used in our experimentation composed of different multimodal medical images of complex nature. Each modality of the image represents information of different kind. In the fusion process, we can combine information of same or different modalities into a single composite image which is information rich and hence suitable for better diagnosis. For performing the fusion process, it is mandatory that images to be used should be registered, if not, their fusion may yield inaccurate results. However, image registration itself is a wide topic, and out of scope of this work. Hence, in the proposed work, we have taken pre-registered source images.

5.2 Experimental results

The fusion results of the proposed method and other methods used in comparison have been presented in this section. We have presented results in visual, tabular and graphical forms. We have compared the proposed method with several well established fusion methods based on both spatial and wavelet domain. Spatial domain methods (PCA [9] and sharp fusion [31]) and, transform domain methods (LP [14], SWT [32], DWT [33], DTCWT [34], LWT [35], MWT [36], DCxWT [22] and NSCT [25]) have been used in comparison. The visual results of the proposed and the other methods [9, 14, 22, 25, 32–36] for the ten sets of medical images are shown in Figs. 4–13.

The human eyes have its own limitations; therefore, if the difference in image quality is very small then, it is difficult to decide which image is better in terms of image content. Hence, we have extended our analysis to quantitative evaluation. To evaluate the performance of the proposed method quantitatively, we were used five image fusion quality measures – entropy, standard deviation, edge strength, sharpness and average gradient. Values of these measurements, for the proposed method and other state-of-the-art methods, used in comparison are tabulated in Tables 1–10, corresponding to all the ten sets of medical images used in our experiments. The best results in each table are highlighted in bold face.

For better comparison of the fusion performance of the proposed method, we have plotted fusion metric values in form of bar charts. For the representative purpose, plots of entropy, sharpness and average gradient have been given in Figs. 14–16, respectively. In Fig. 14*a*, comparison of the proposed method with PCA [9], SHARP [31], LP [14], SWT [32] and DWT [33] has been shown whereas in Fig. 14*b*, comparison of the proposed method with the methods DTCWT [34], LWT [35], MWT [36], DCxWT [22] and NSCT [25] has been shown in terms of entropy values for the source images shown in Figs. 4–8. In Figs. 14*c* and *d*, comparison of the proposed method with other state-of-the-art methods [9, 14, 22, 25, 31–36] has been given for the source images shown in Figs. 9–13. Similar comparisons have been presented in Figs. 15 and 16 for the sharpness and average gradient values, respectively. These metric values are plotted for all the ten sets of medical images used in our experiments.

We could clearly observe from Figs. 14*a–d*, that in most of the cases, the proposed method has better entropy values than the other methods used in comparison. It is clear from the Figs. 15 and 16

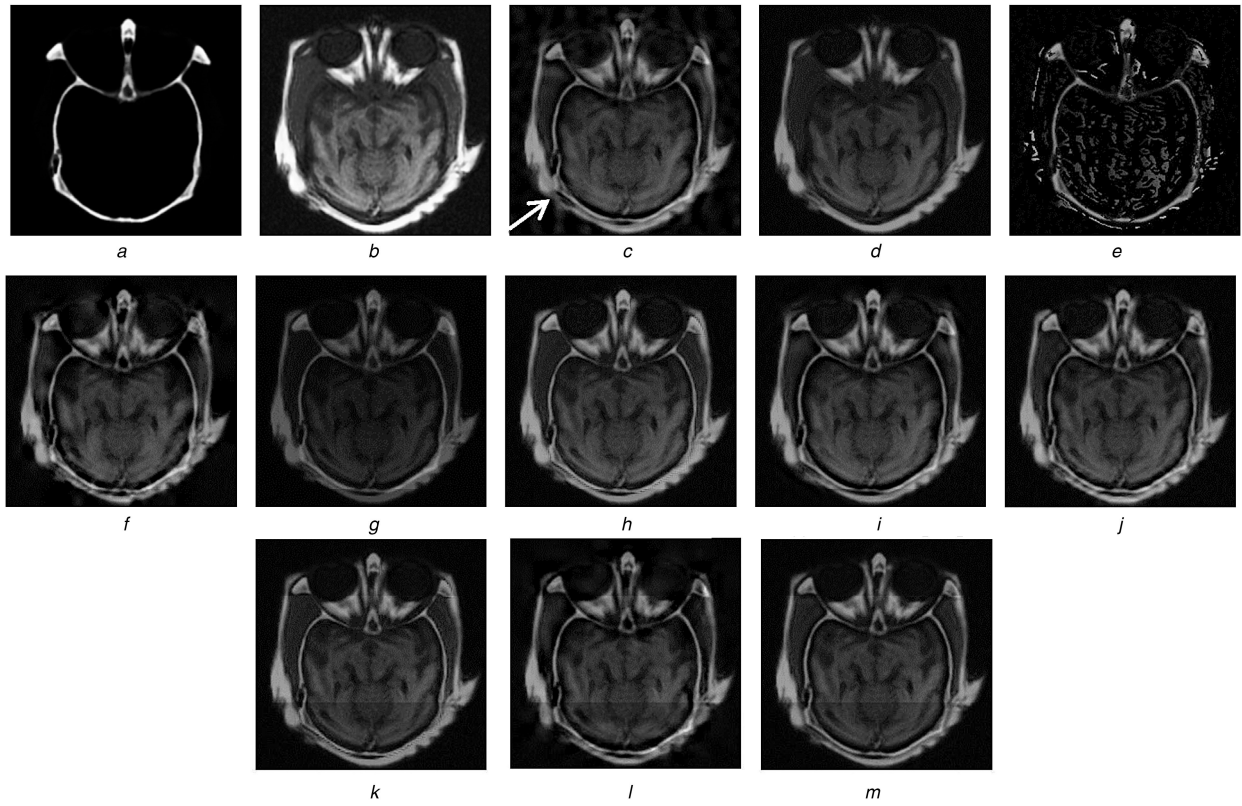


Fig. 5 Fusion results of second set of medical images. *a* and *b* are source images

a CT image

b MRI image

c–m Fusion results of the proposed and other methods. Better visual structure can be easily observed at the region indicated by an arrow

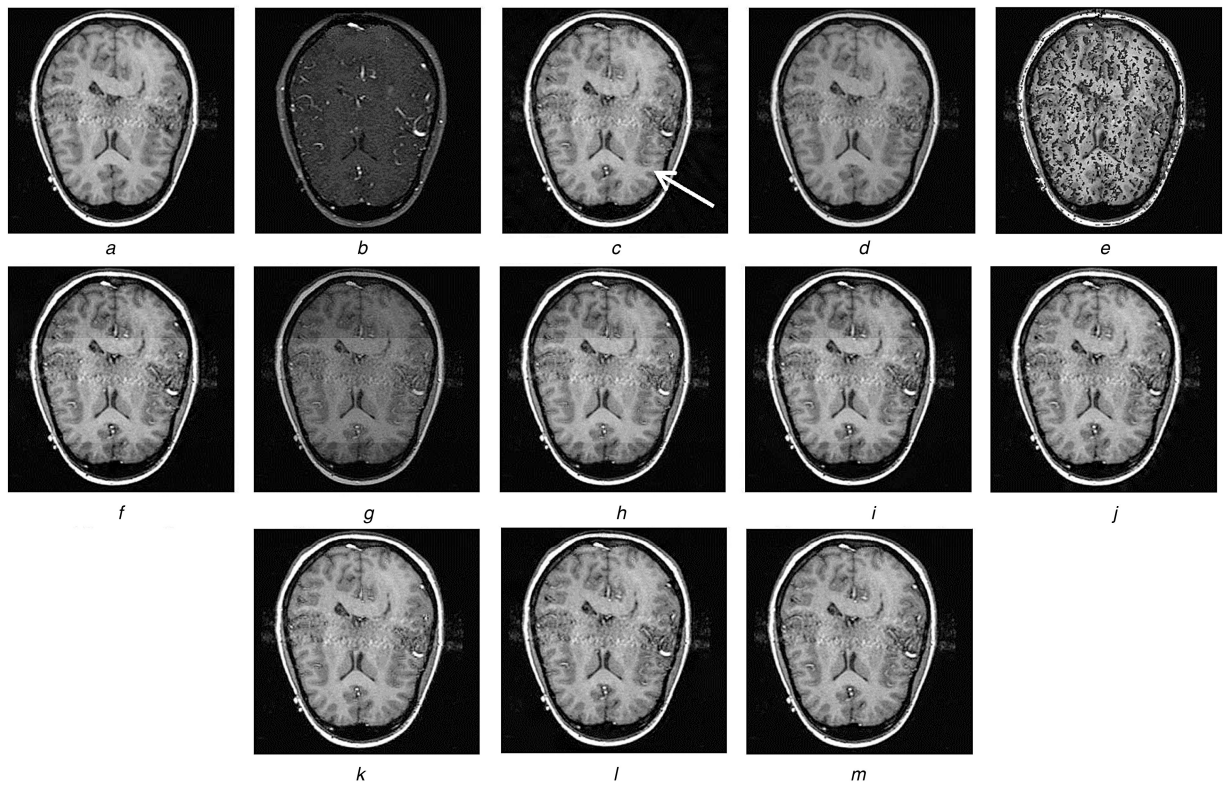


Fig. 6 Fusion results of third set of medical images. *a* and *b* are source images

a T1-MRI image

b MRA image

c–m Fusion results of the proposed and other methods. Better visual structure can be easily observed at the region indicated by an arrow

that PCA [9] and SHARP [31] fusion methods resulted in higher sharpness and average gradient values, but from visual results one can see that these methods could not retain all relevant information

of the source images in the fused image and thus reducing the image quality.

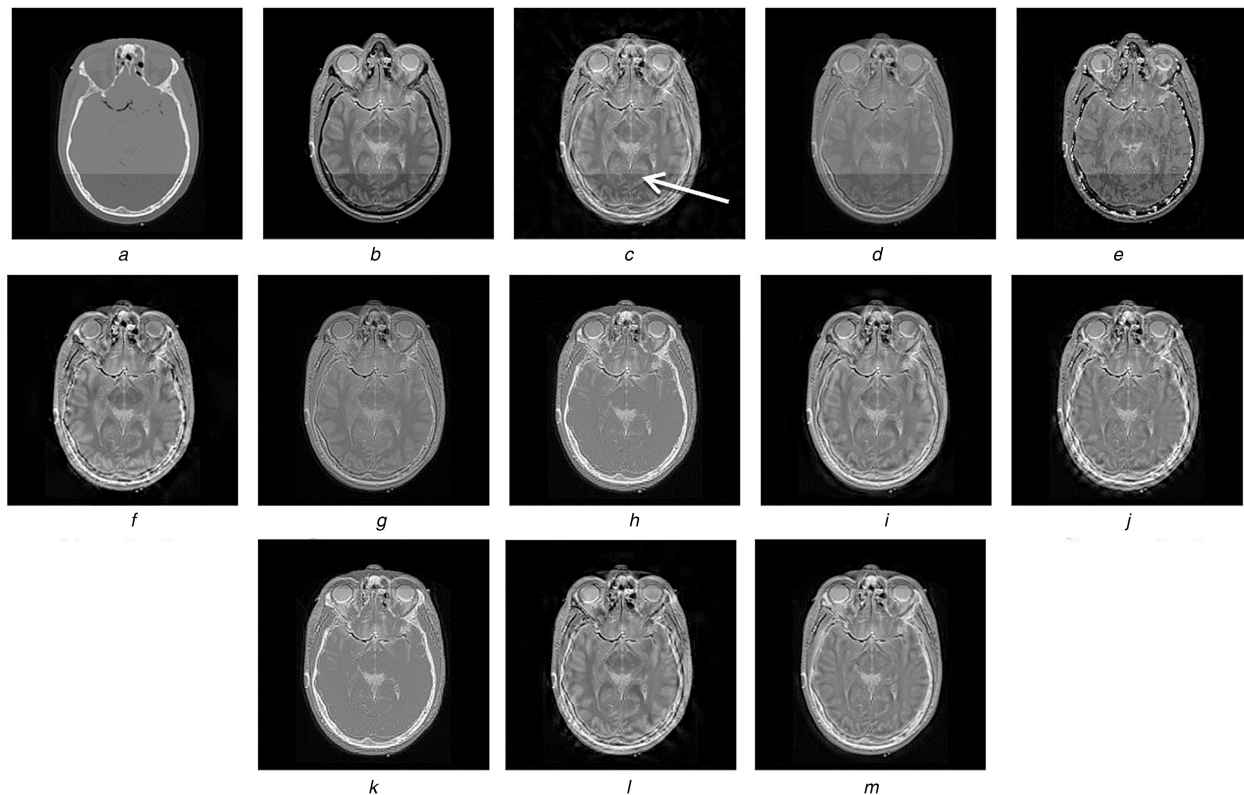


Fig. 7 Fusion results of fourth set of medical images. *a* and *b* are source images

a CT image

b MRI image

c–m Fusion results of the proposed and other methods. Better visual structure can be easily observed at the region indicated by an arrow

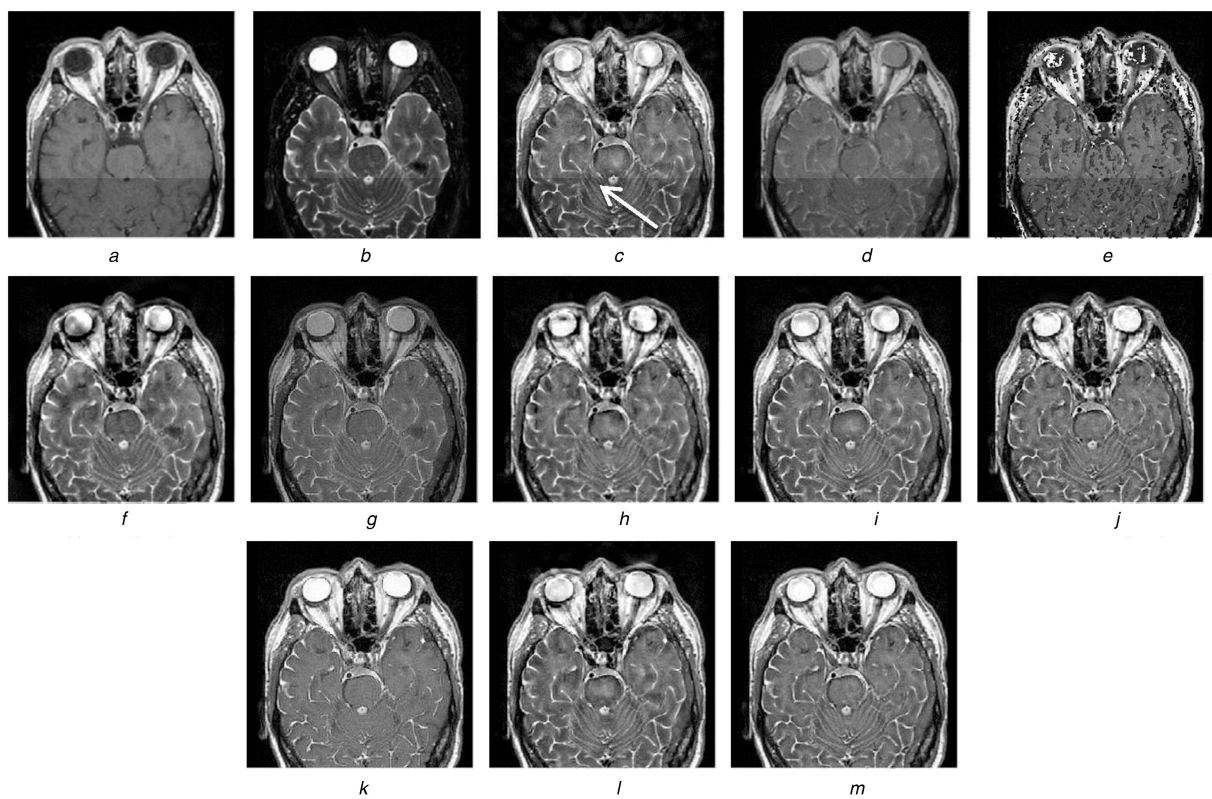


Fig. 8 Fusion results of fifth set of Medical images. *a* and *b* are source images

a T1-weighted MRI image

b T2-weighted MRI image

c–m Fusion results of the proposed and other methods. Better visual structure can be easily observed at the region indicated by an arrow

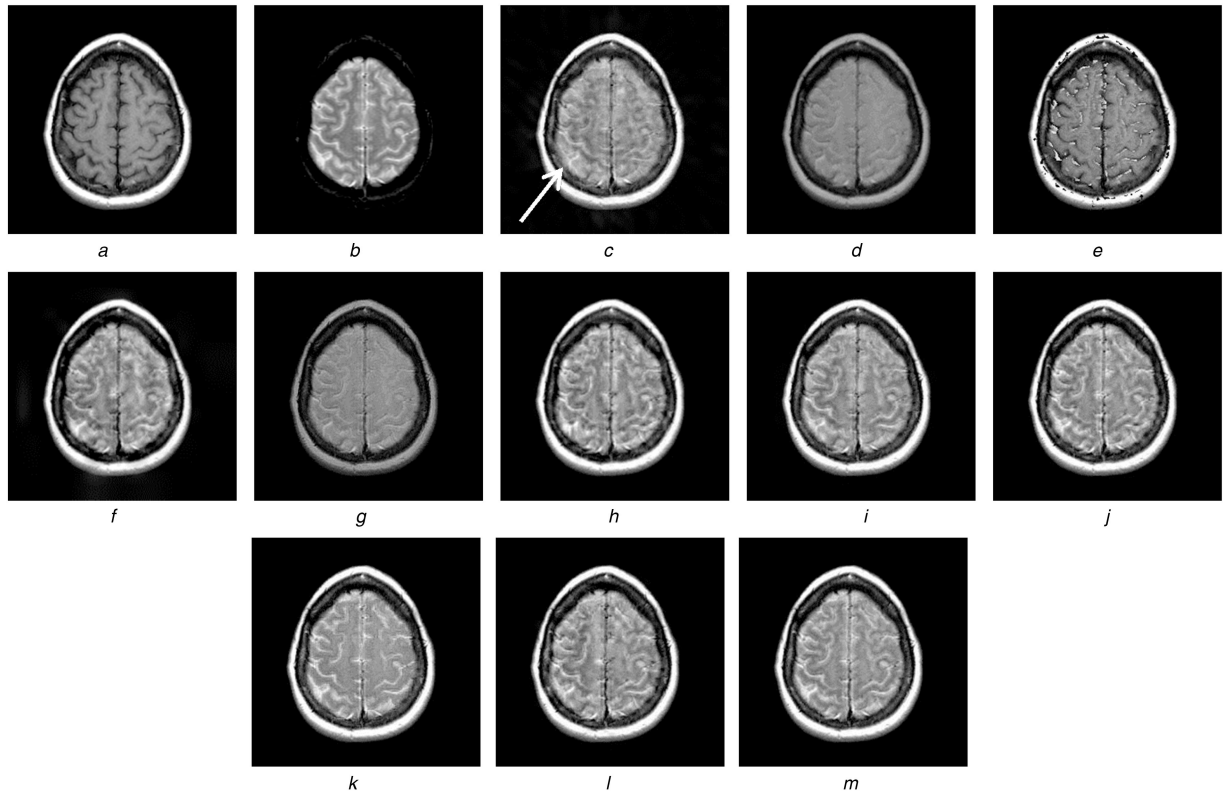


Fig. 9 Fusion results of sixth set of Medical images. *a* and *b* are source images

a T1-weighted MRI image

b T2-weighted MRI image

c–*m* Fusion results of the proposed and other methods. Better visual structure can be easily observed at the region indicated by an arrow

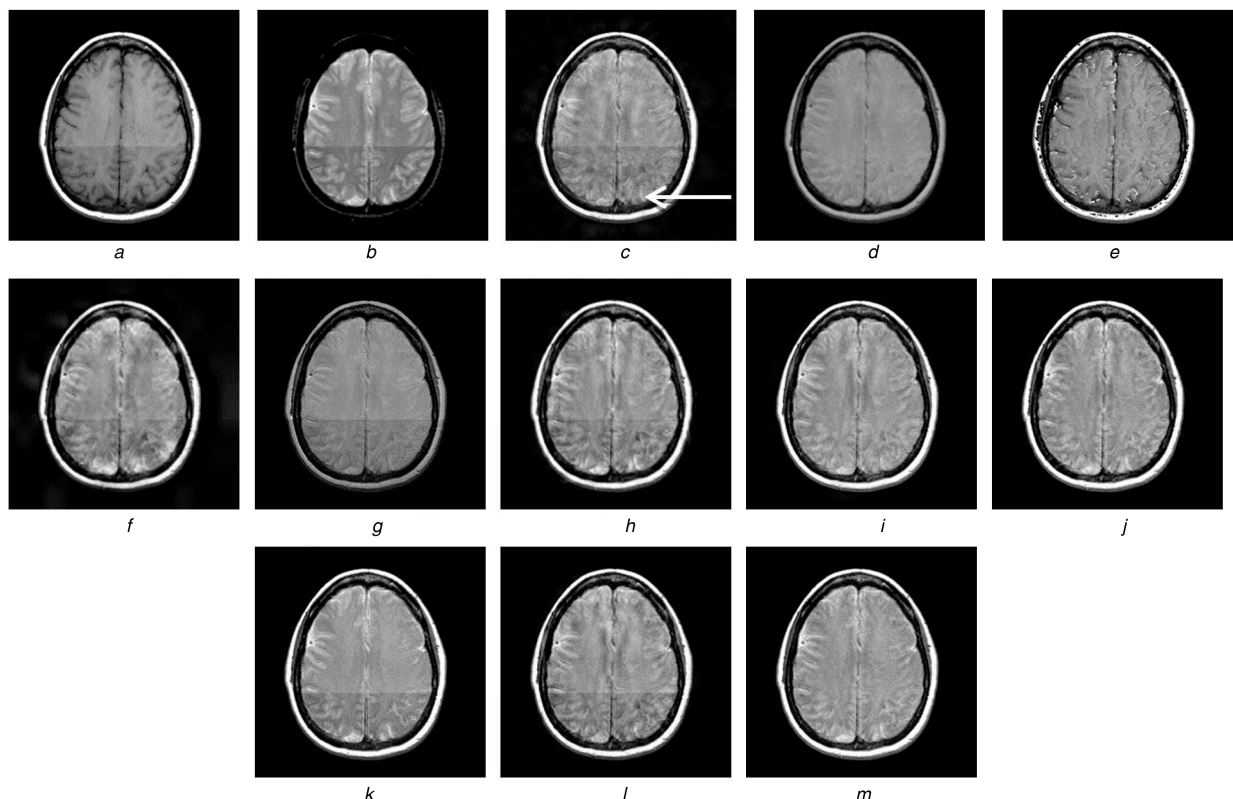


Fig. 10 Fusion results of seventh set of Medical images. *a* and *b* are source images

a T1-weighted MRI image

b T2-weighted MRI image

c–*m* Fusion results of the proposed and other methods. Better visual structure can be easily observed at the region indicated by an arrow

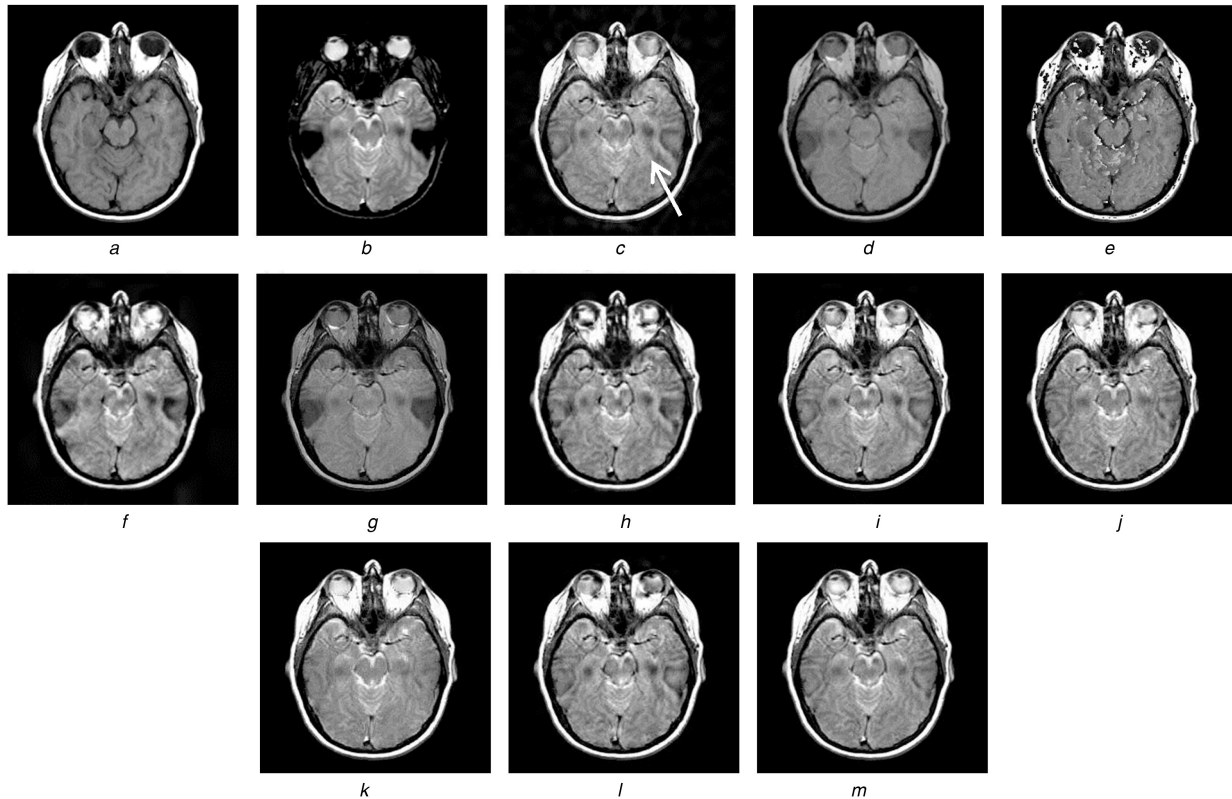


Fig. 11 Fusion results of eighth set of medical images. *a* and *b* are source images

a T1-weighted MRI image

b T2-weighted MRI image

c–*m* Fusion results of the proposed and other methods. Better visual structure can be easily observed at the region indicated by an arrow

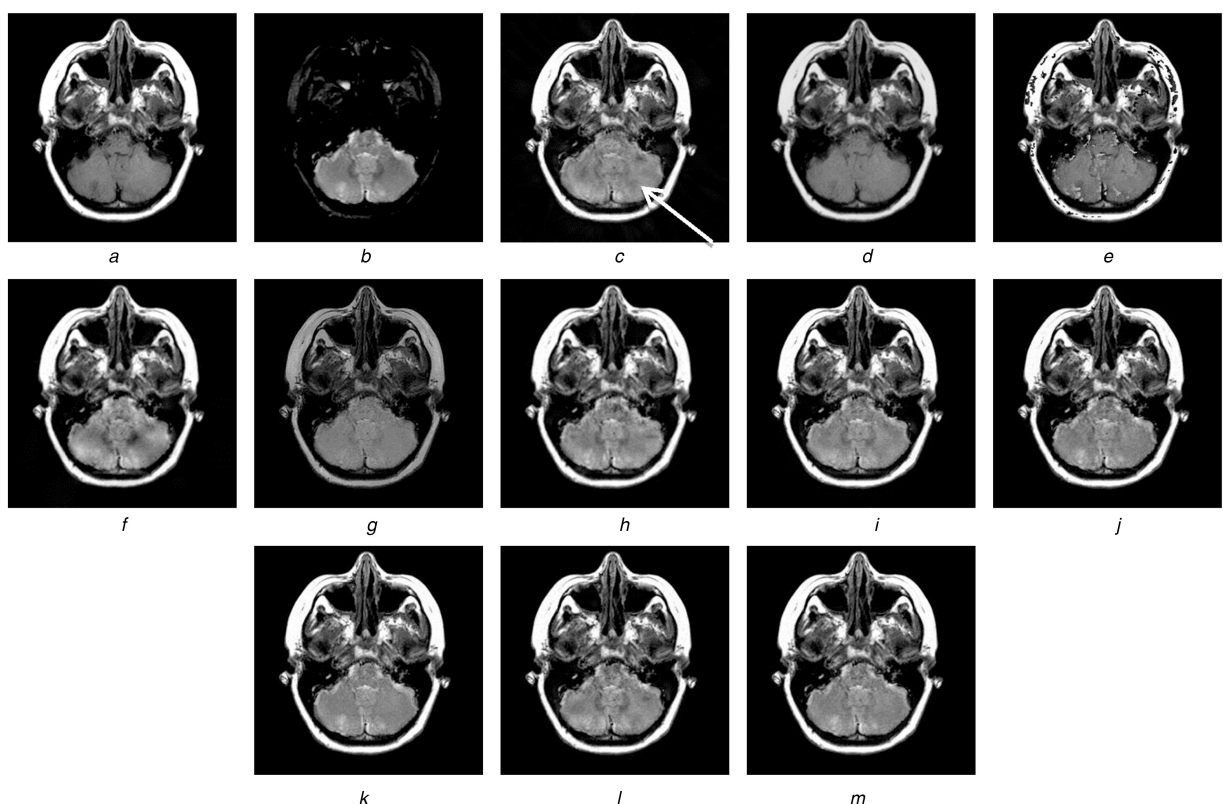


Fig. 12 Fusion results of ninth set of medical images. *a* and *b* are source images

a T1-weighted MRI image

b T2-weighted MRI image

c–*m* Fusion results of the proposed and other methods. Better visual structure can be easily observed at the region indicated by an arrow

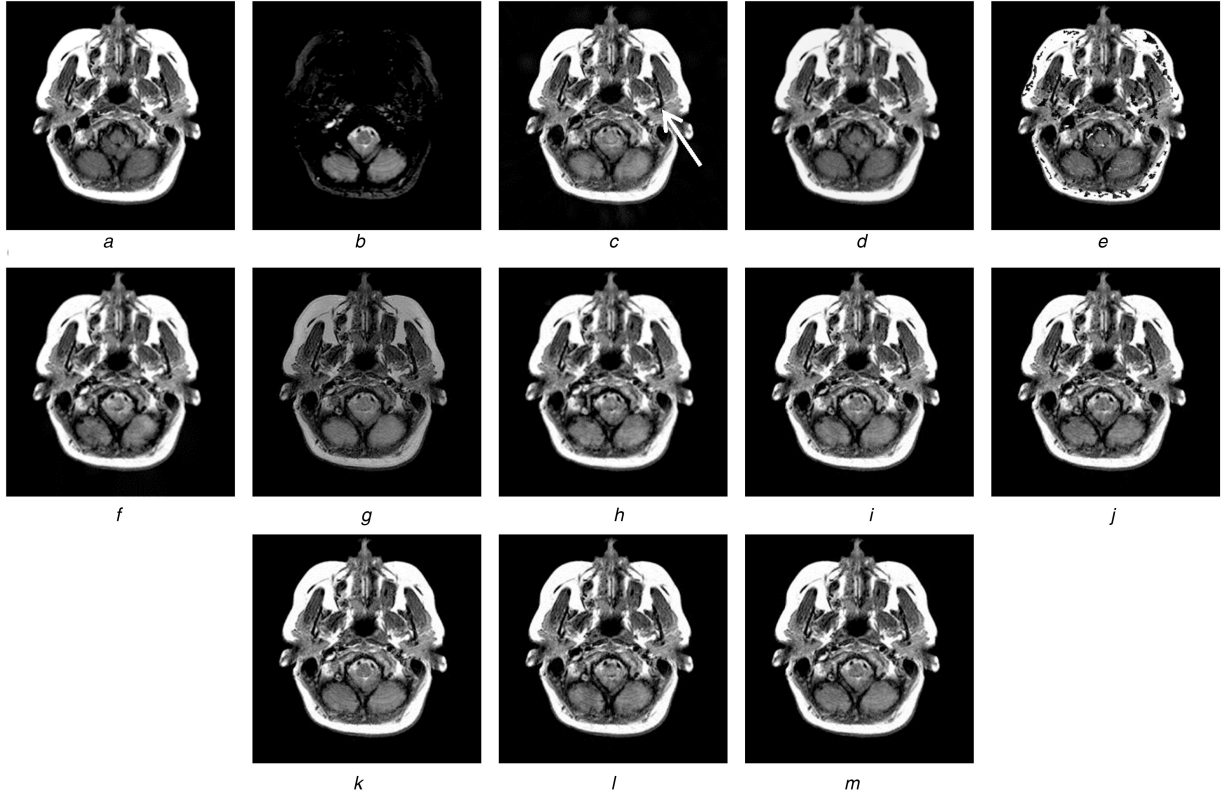


Fig. 13 Fusion results of tenth set of medical images. *a* and *b* are source images

a T1-weighted MRI image

b T2-weighted MRI image

c–m Fusion results of the proposed and other methods. Better visual structure can be easily observed at the region indicated by an arrow

5.3 Observations, analyses and discussion

Observation 1: From Tables 1–10, it can be observed that the proposed method has the higher entropy values in 1st, 3rd, 4th, 9th and 10th set of source images (Tables 1, 3, 4, 9 and 10), LP [14] resulted higher entropy values in 5th, 6th, 7th and 8th set of source images (Tables 5–8), and DCxWT [22] in 2nd set of source image (Table 2). An important fact is that the LP- and DCxWT-based methods resulted entropy values very close to that of the proposed method (Fig. 14). However, visual results for the proposed method are close to the DCxWT-based method [22] and better than the other methods (Figs. 4–10) used in the comparison. On the other hand, we could see from Fig. 14, that the LP [14] fusion has higher entropy for 6th, 7th and 8th image sets, but these methods introduce blur at the same time making the fused image of poor quality.

Table 1 Quantitative assessments of different fusion methods on the source images shown in Figs. 4*a* and *b*

Methods	Entropy	Standard deviation	Q_{AB}^F	Sharpness	Average gradient
proposed	5.586283	63.407743	0.719627	6.268876	5.785534
PCA [9]	4.970669	60.659414	0.584586	4.018290	3.600045
SHARP [31]	5.398629	74.552405	0.513791	18.204664	17.280266
LP [14]	5.250549	63.501639	0.739492	6.247827	5.760611
SWT [32]	5.032116	60.802633	0.637705	4.610195	4.154916
DWT [33]	5.192241	63.590862	0.710567	6.279833	5.789174
DTCWT [34]	5.119788	63.616116	0.754177	6.236733	5.755415
LWT [35]	5.203715	64.027483	0.708257	6.220029	5.737093
MWT [36]	5.085785	64.485881	0.601475	5.743939	5.248007
DCxWT [22]	5.183401	63.549891	0.742579	6.254366	5.767501
NSCT[25]	5.114117	63.985589	0.740254	6.015021	5.541361

Observation 2: From Tables 1–10 and Fig. 15, we could see that the proposed method has sharpness values smaller than the method SHARP [31] (Figs. 15*a* and *c*), similar to PCA [9] and DWT [33], and higher than the methods LP [14], SWT [32], MWT [36], DTCWT [34] and LWT [35] (Figs. 15*c* and *d*). Also, from the visual analysis, we observe that, in most of the cases (Figs. 4–13) spatial domain (PCA [9] and SHARP [31]) based methods yield poor fusion results in comparison to the proposed method. The poor performance of spatial domain methods can be well observed in Fig. 4 (edges are blurred in the fused image) even though sharpness values are higher. LP [14], DWT [32] and SWT [33] methods resulted a little improvement in fusion performance over SHARP [31] and PCA [9] methods. SWT [32], DWT [33] and MWT [36] based fusion have still poor visual results. Though DTCWT [34], DCxWT [22] and NSCT [25] have better visual quality and comparable sharpness values (Tables 6–10 and Fig. 15*d*).

Observation 3: From Tables 1–10 and Fig. 16, we could see that the average gradient values for the proposed method are smaller than the SHARP [31] method for almost all image sets, similar to LP [14], DWT [25] and higher than PCA [9] and SWT [33] for almost all set of source images (Figs. 16*a* and *c*). On the other hand, the methods based on LWT [35], DTCWT [34], SWT [33], DCxWT [22] and NSCT [25] have shown similar performance (Figs. 16*b* and *d*) for all image sets except the image set 4 in which SWT [33] has very high value of average gradient.

Observation 4: From Tables 1–10, we have also observed that the methods wavelet transform-based methods (SWT [32], MWT [36] and DCxWT [22]) resulted in higher standard deviation than the proposed method. While edge strength values resulted in our experiments were little higher for the MWT [36] based method in most of the cases (Tables 4, 6–10). Whereas DTCWT [34] has higher value in two sets of images (Tables 1 and 2), and PCA [9] in one case (Table 3). However, the values for this metric on any image sets are very close to each other and similar to the proposed method too. This shows that in terms of this metric one cannot judge the quality of fused images in our results. To make the final decision, we have critically analysed the visual results. The

combined analysis leads to a conclusion that the proposed method has comparative performance to that of DCxWT (Figs. 1–10) and better performance over other methods (Figs. 1–10). This is due to the multidirectional and better edge representation capability of the curvelet transform.

Discussion: Observation 1 shows that the entropy values are high for the proposed method for most of the set of source images. Entropy is the measure of information content of the image, resulting in information enriched fused image. Although in some

Table 2 Quantitative assessments of different fusion methods on the source images shown in Figs. 5a and b

Methods	Entropy	Standard deviation	Q_{AB}^F	Sharpness	Average gradient
proposed	5.693754	60.593411	0.500984	7.971973	7.638686
PCA [9]	4.613887	51.663547	0.372180	4.153375	3.984863
SHARP [31]	4.851961	53.273605	0.517973	8.533343	8.100653
LP [14]	5.801392	60.503028	0.495168	8.103338	7.750777
SWT [32]	5.031475	51.828796	0.499613	6.373672	6.073065
DWT [33]	5.280746	61.912005	0.541031	7.906643	7.563040
DTCWT [34]	5.479103	60.466511	0.567474	7.640822	7.311915
LWT [35]	5.438992	61.746718	0.493166	8.363953	8.019561
MWT [36]	5.261636	61.922750	0.522606	7.805822	7.470271
DCxWT [22]	5.914910	59.634730	0.508618	8.188739	7.843382
NSCT[25]	5.417293	61.232277	0.590439	7.807120	7.464963

Table 3 Quantitative assessments of different fusion methods on the source images shown in Figs. 6a and b

Methods	Entropy	Standard deviation	Q_{AB}^F	Sharpness	Average gradient
proposed	6.684740	67.164802	0.565923	9.299422	9.052734
PCA [9]	5.704395	56.574647	0.654891	6.833020	6.677453
SHARP [31]	5.889100	61.707860	0.455984	16.298692	15.561676
LP [14]	6.361303	67.643440	0.590535	9.498035	9.236607
SWT [32]	5.512988	44.022285	0.511997	6.654302	6.450173
DWT [33]	5.927999	5.927999	0.640343	9.422617	9.181926
DTCWT [34]	6.266344	67.399337	0.613544	9.260559	9.023898
LWT [35]	6.158698	67.865454	0.579072	9.717206	9.460907
MWT [36]	5.964454	67.636215	0.637334	9.470049	9.198334
DCxWT [22]	6.110119	32.205116	0.640980	4.161012	4.082677
NSCT[25]	6.106631	67.516315	0.623846	9.325269	9.084947

Table 4 Quantitative assessments of different fusion methods on the source images shown in Figs. 7a and b

Methods	Entropy	Standard deviation	Q_{AB}^F	Sharpness	Average gradient
proposed	6.327028	31.436995	0.578114	4.061086	3.994742
PCA [9]	5.621955	28.455679	0.639548	2.856569	2.794581
SHARP [31]	3.059175	23.732274	0.300643	5.563211	5.199172
LP [14]	6.212811	33.114610	0.601387	4.123783	4.045845
SWT [32]	5.204857	18.861420	0.447260	2.316577	2.261096
DWT [33]	5.858703	32.961944	0.772153	4.152217	4.071535
DTCWT [34]	6.099878	31.894921	0.695092	3.997509	3.922969
LWT [35]	5.996785	32.667652	0.703852	4.121661	4.053019
MWT [36]	5.874340	32.914727	0.774094	3.992424	3.912414
DCxWT [22]	6.223833	67.488540	0.590151	9.517875	9.253037
NSCT[25]	5.957256	32.555556	0.766557	4.003977	3.932055

cases, its value is a little smaller for the proposed method in comparison to other methods, but visual results have shown the better structures in fused image. From observation 2, it could be found that PCA and SHARP fusion methods have better sharpness values, but could not present clear edge structure in the fused images. Although DTCWT [34], DCxWT [22] and NSCT [25] based fusion methods produce better visual results, but slightly poorer than the proposed method. This is due to the high directional edge representation of the curvelet transform. However, in observation 3, we could see that the average gradient values are maximum for SHARP [31] fusion. Gradient values indicate how small changes in image content are retained in fused image. From observation 4, we could see that in some cases DCxWT [22] based method perform better than the other methods, but compared to the proposed method. Combining observations 1–4 and based on the visual and quantitative analysis, we found that PCA [9] and SHARP [31] methods could produce blur in the fused images, LP [14] and LWT [35] based fusion have slight improvement in the image quality, whereas SWT [32], DWT [33] and MWT [36] based fusion methods still give poorer visual results. Though DTCWT [34], DCxWT [22] and NSCT [25] based methods have better visual quality results in comparison to other methods, but quite similar to the proposed method. Overall evaluations of the results for medical image fusion have shown better performance of the proposed method over other methods (PCA [9], SHARP [31], LP [14], SWT [32], DTCWT [34], DCxWT [22] and NSCT [25]). The outperformance of the proposed method is benefitted by the better edge representation and higher directional selectivity nature of the curvelet transform.

6 Conclusions

Combining the information from different multimodal medical images to a single fused image has been performed. The medical image fusion results information enriched image which is suitable for the diagnosis of abnormalities in the human body. In this paper, we have proposed a curvelet transform-based method for fusion of medical images using local energy-based fusion rule. The flexible directionality, anisotropy and needle-shaped basis elements used in the computation of curvelet transform, makes it more powerful for image fusion. Finer details in the medical images can be well recognised due to the high edge capturing strength of the curvelet transform. Local energy-based fusion rule used in our fusion method, improves the quality of fused image by considering the neighbouring coefficients besides the centre coefficient for the selection of fused coefficients. In addition, it reduces the chance of selection of noisy coefficient and improves the quality of edges in the fused image. The performance of the proposed method has been evaluated visually and quantitatively and we compared it with other well established fusion methods viz. spatial, pyramidal, wavelet and contourlet domain-based fusion methods. The outperformance of the proposed method has been observed. For quantitative evaluation, we used five metrics (entropy, standard deviation, edge strength, sharpness and average gradient). The representative results on ten pair of medical images have shown the improved performance over other methods used in comparison.

Table 5 Quantitative assessments of different fusion methods on the source images shown in Figs. 8a and b

Methods	Entropy	Standard deviation	Q_{AB}^F	Sharpness	Average gradient
proposed	7.267056	64.992696	0.532126	15.241557	14.338728
PCA [9]	6.650282	47.459965	0.443446	8.783408	8.249183
SHARP [31]	6.880298	60.006877	0.408923	18.438314	17.160081
LP [14]	7.323847	64.202704	0.546688	15.502308	14.579093
SWT [32]	6.766220	44.964728	0.446422	11.982232	11.113891
DWT [33]	7.201451	66.666538	0.549169	16.360911	15.407146
DTCWT [34]	7.204609	65.944450	0.602191	15.396372	14.495069
LWT [35]	7.134114	67.493453	0.550820	16.182151	15.243621
MWT [36]	7.097230	67.042506	0.568070	15.638207	14.727125
DCxWT [22]	7.307347	65.916516	0.556448	15.800089	14.872447
NSCT[25]	7.151873	66.892703	0.607225	15.472105	14.572932

Table 6 Quantitative assessments of different fusion methods on the source images shown in Figs. 9a and b

Methods	Entropy	Standard deviation	Q_{AB}^F	Sharpness	Average gradient
proposed	5.534005	69.850492	0.541651	6.657009	6.506858
PCA [9]	3.630611	52.172051	0.439472	3.736291	3.656144
SHARP [31]	3.436556	64.154082	0.601885	8.065580	7.751982
LP [14]	5.699046	68.724920	0.544048	6.749879	6.589254
SWT [32]	3.773703	51.539546	0.388470	4.373007	4.246020
DWT [33]	4.114684	71.708719	0.557273	7.241534	7.063637
DTCWT [34]	4.319255	70.918462	0.604791	6.562549	6.418164
LWT [35]	3.964762	72.095465	0.581557	6.982702	6.982702
MWT [36]	3.861285	72.639879	0.663696	6.824751	6.661734
DCxWT [22]	4.413063	71.039223	0.572326	6.838707	6.681556
NSCT[25]	3.967112	71.942104	0.628074	6.676487	6.527337

Table 7 Quantitative assessments of different fusion methods on the source images shown in Figs. 10a and b

Methods	Entropy	Standard deviation	Q_{AB}^F	Sharpness	Average gradient
proposed	5.601831	70.846762	0.565808	7.649525	7.425651
PCA [9]	3.834550	57.445443	0.463634	4.392717	4.273259
SHARP [31]	3.834550	57.445443	0.463634	4.392717	4.273259
LP [14]	6.339818	68.868787	0.539681	7.532237	7.301753
SWT [32]	4.097771	57.371376	0.449473	5.517018	5.344157
DWT [33]	4.794561	72.093105	0.569548	8.033314	7.790752
DTCWT [34]	4.788148	71.388871	0.610489	7.463862	7.251414
LWT [35]	4.312342	72.555104	0.592174	7.908199	7.682166
MWT [36]	4.135134	73.087497	0.655931	7.722764	7.493061
DCxWT [22]	4.984435	71.032923	0.570785	7.664480	7.437146
NSCT[25]	4.342521	72.399042	0.632582	7.511989	7.299081

Table 8 Quantitative assessments of different fusion methods on the source images shown in Figs. 11a and b

Methods	Entropy	Standard deviation	Q_{AB}^F	Sharpness	Average gradient
proposed	6.116058	76.289296	0.537630	10.186916	9.873831
PCA [9]	4.337418	55.601989	0.488971	5.960802	5.782740
SHARP [31]	3.905315	69.692292	0.537627	11.886631	11.364064
LP [14]	6.415730	74.108674	0.516578	9.840640	9.518282
SWT [32]	4.637718	54.049384	0.447205	7.329014	7.077040
DWT [33]	5.114226	77.241864	0.539247	10.519138	10.177471
DTCWT [34]	5.333055	76.332101	0.594601	9.896573	9.600042
LWT [35]	4.784136	78.185362	0.515362	10.491411	10.171205
MWT [36]	4.570202	78.733077	0.633487	10.195644	9.872423
DCxWT [22]	5.554382	75.917717	0.549922	9.964478	9.648679
NSCT[25]	4.868040	77.578805	0.615112	9.979263	9.681540

Table 9 Quantitative assessments of different fusion methods on the source images shown in Figs. 12a and b

Methods	Entropy	Standard deviation	Q_{AB}^F	Sharpness	Average gradient
proposed	5.461620	75.149902	0.718110	9.718110	9.171174
PCA [9]	3.874097	64.919201	0.758107	7.379621	7.167478
SHARP [31]	3.484112	71.002447	0.699549	11.238953	10.757000
LP [14]	5.370506	74.583189	0.705271	9.237474	8.963270
SWT [32]	4.241458	45.964968	0.495553	6.648617	6.430424
DWT [33]	4.626619	75.670882	0.719419	9.493849	9.203543
DTCWT [34]	4.691200	75.489322	0.747271	9.303275	9.037288
LWT [35]	4.269511	76.320912	0.731212	9.676697	9.399607
MWT [36]	3.975618	76.413576	0.776511	9.457726	9.183833
DCxWT [22]	4.815141	75.195892	0.718642	9.311155	9.035167
NSCT[25]	4.312483	75.767839	0.757709	9.345787	9.078416

Table 10 Quantitative assessments of different fusion methods on the source images shown in Figs. 13a and b

Methods	Entropy	Standard deviation	Q_{AB}^F	Sharpness	Average gradient
proposed	5.466256	80.259348	0.749960	9.747650	9.458297
PCA [9]	4.002249	76.291784	0.800507	8.668355	8.412958
SHARP [31]	3.643111	77.075498	0.719239	12.202747	11.713124
LP [14]	5.041733	80.115464	0.747769	9.666738	9.368834
SWT [32]	4.349691	44.596162	0.521899	6.946983	6.712987
DWT [33]	4.499056	80.583972	0.741245	9.852128	9.548420
DTCWT [34]	4.360988	80.612908	0.777703	9.706423	9.420643
LWT [35]	4.319099	81.248754	0.760541	10.043043	9.746083
MWT [36]	4.124530	81.250543	0.798699	9.925776	9.626970
DCxWT [22]	4.510346	80.475058	0.755069	9.702227	9.405492
NSCT[25]	4.318138	80.751918	0.788945	9.781620	9.494088

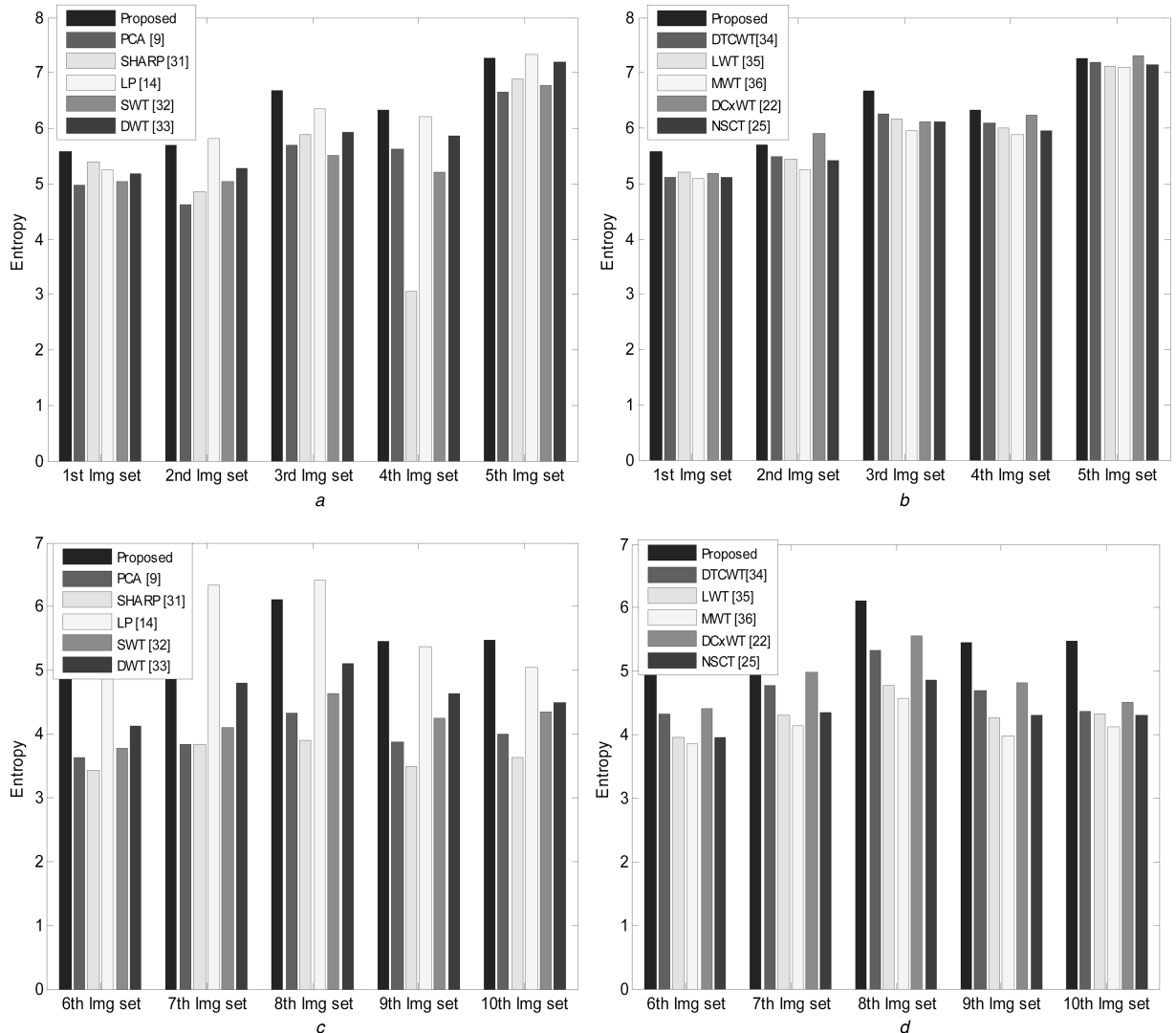


Fig. 14 Comparative performance in terms of entropy of the fused images

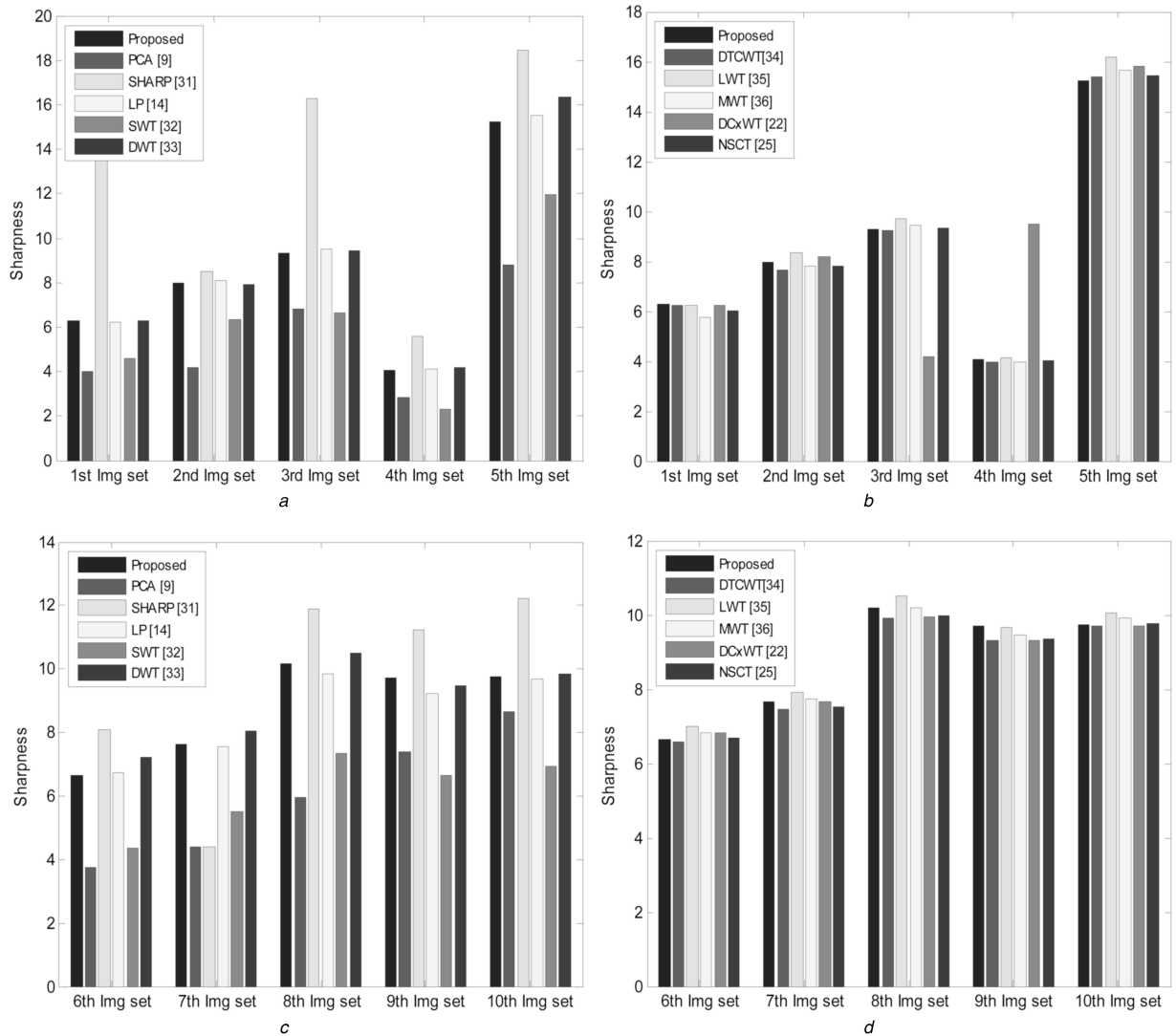


Fig. 15 Comparative performance in terms of sharpness of the fused images

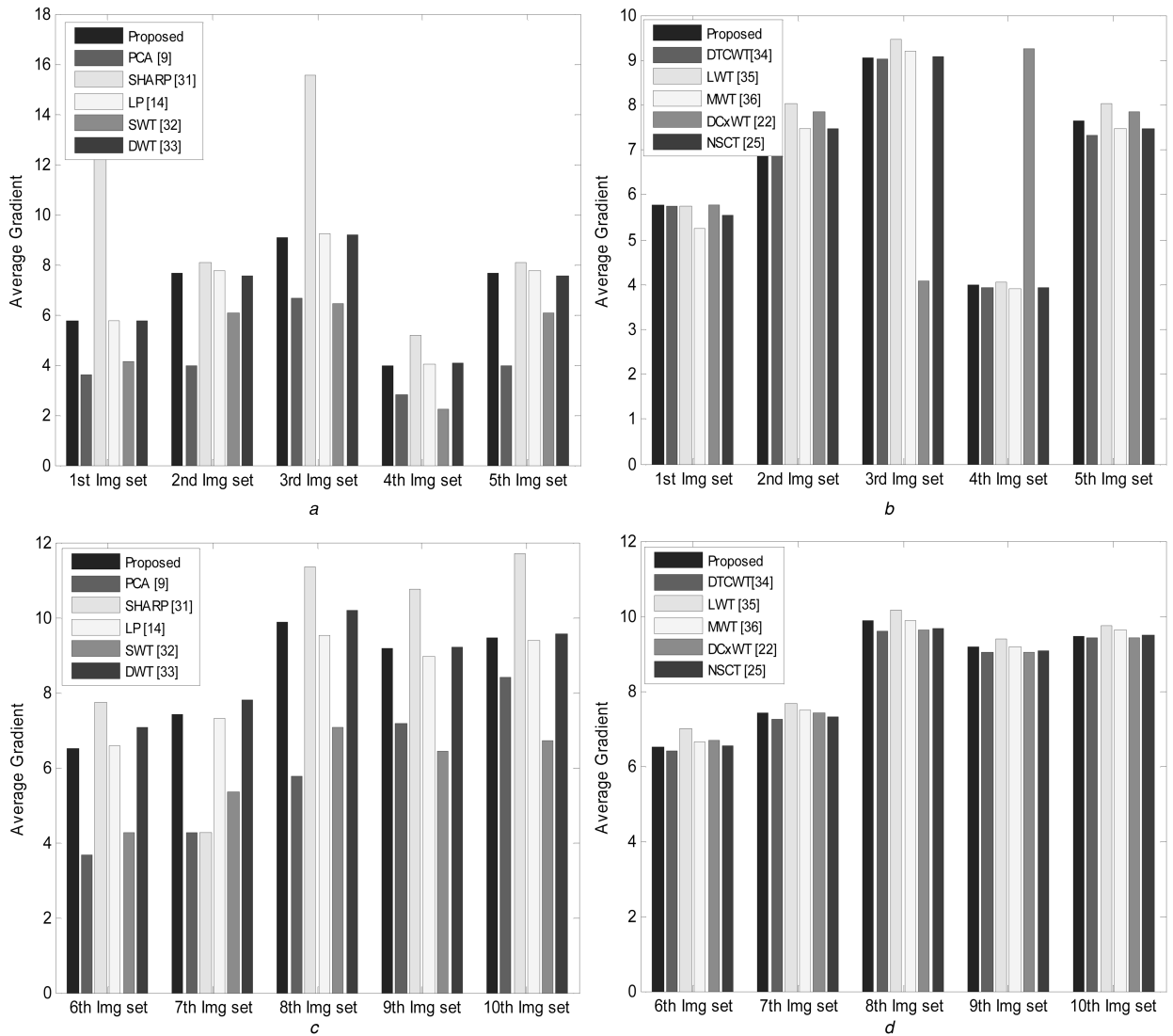


Fig. 16 Comparative performance in terms of average gradient of the fused images

7 References

- [1] James, A.P., Dasarathy, B.V.: ‘Medical image fusion: a survey of the state-of-the-art’, *Inf. Fusion*, 2014, **19**, pp. 4–19
- [2] Barra, V., Boire, J.V.: ‘A general framework for the fusion of anatomical and functional medical images’, *NeuroImage*, 2001, **13**, (3), pp. 410–424
- [3] Khare, A., Tiwari, U.S.: ‘Soft-thresholding for denoising of medical images—A multiresolution approach’, *Int. J. Wavelets, Multiresolution Inf. Process.*, 2005, **3**, (4), pp. 477–496
- [4] Khare, A., Tiwari, U.S., Jeon, M.: ‘Daubechies complex wavelet transform based multilevel shrinkage for deblurring of medical images in presence of noise’, *Int. J. Wavelets, Multiresolution Inf. Process.*, 2009, **7**, (5), pp. 587–604
- [5] Khalegi, B., Khamis, A., Karray, F.O., et al.: ‘Multisensor data fusion: a review of the state-of-the-art’, *Inf. Fusion*, 2013, **14**, (1), pp. 28–44
- [6] Yang, B., Li, S.: ‘Pixel level image fusion with simultaneous orthogonal matching pursuit’, *Inf. Fusion*, 2012, **13**, (1), pp. 10–19
- [7] Yang, J., Zang, X.: ‘Feature-level fusion of fingerprint and finger-vein for personal identification’, *Pattern Recognit. Lett.*, 2012, **33**, (5), pp. 623–628
- [8] Tao, Q., Veldhuis, R.: ‘Threshold-optimized decision-level fusion and its application to biometrics’, *Pattern Recognit.*, 2009, **42**, (5), pp. 823–836
- [9] Wan, T., Zhu, C., Qin, Z.: ‘Multifocus image fusion based on robust principal component analysis’, *Pattern Recognit. Lett.*, 2013, **34**, (9), pp. 1001–1008
- [10] Burt, P.J., Adelson, E.H.: ‘The laplacian pyramid as a compact image code’, *IEEE Trans. Commun.*, 1983, **31**, (4), pp. 532–540
- [11] Li, H., Manjunath, B.S., Mitra, S.K.: ‘Multisensor image fusion using wavelet transform’, *Graph. Models Image Process.*, 1995, **57**, (3), pp. 235–245
- [12] Nehcini, F., Garzelli, A., Baronti, S., et al.: ‘Remote sensing image fusion using the curvelet transform’, *Inf. Fusion*, 2007, **8**, (2), pp. 143–156
- [13] Li, S., Yang, B.: ‘Multifocus image fusion by combining curvelet and wavelet transform’, *Pattern Recognit. Lett.*, 2008, **29**, (9), pp. 1295–1130
- [14] Wang, W., Chang, F.: ‘A multi-focus image fusion method based on Laplacian pyramid’, *J. Comput.*, 2011, **6**, (12), pp. 2559–2566
- [15] Candes, E.J., Donoho, D.L.: ‘Continuous curvelet transform: I. Resolution of the wavefront set’, *Appl. Comput. Harmon. Anal.*, 2005, **19**, (2), pp. 162–197
- [16] Candes, E.J., Donoho, D.L.: ‘Continuous curvelet transform: II. Discretization and frames’, *Appl. Comput. Harmon. Anal.*, 2005, **19**, (2), pp. 198–222

- [17] Candes, E., Demanet, L., Donoho, D., *et al.*: ‘Fast discrete curvelet transforms’, *Multiscale Model. Simul.*, 2006, **5**, (3), pp. 861–899
- [18] Binh, N.T., Khare, A.: ‘Multilevel threshold based image denoising in curvelet domain’, *J. Comput. Sci. Technol.*, 2010, **25**, (3), pp. 632–640
- [19] Binh, N.T., Khare, A.: ‘Object tracking of video sequences in curvelet domain’, *Int. J. Image Graph.*, 2011, **11**, (1), pp. 1–20
- [20] Khare, M., Srivastava, R.K., Khare, A., *et al.*: ‘Curvelet transform based moving object segmentation’. Proc. of 20th IEEE Int. Conf. on Image Processing (ICIP 2013), Melbourne, Australia, September 2013, pp. 4079–4083
- [21] Mahyari, A.G., Yazdi, M.: ‘A novel image fusion method using curvelet transform based on linear dependency test’. Proc. Int. Conf. Digital Image Processing, Bangkok, Thailand, March 2009, pp. 351–354
- [22] Singh, R., Khare, A.: ‘Fusion of multimodal medical images using Daubechies complex wavelet transform – a multiresolution approach’, *Inf. Fusion*, 2014, **19**, pp. 49–60
- [23] Srivastava, R., Singh, R., Khare, A.: ‘Fusion of multifocus noisy images using contourlet transform’. Proc. 6th Int. Conf. Contemporary Computing, Noida, India, August 2013, pp. 497–502
- [24] Donoho, D.L., Flesia, A.G.: ‘Digital ridgelet transform based on true ridge functions’. in Stocekler, J., Welland, G.V. (Eds.): ‘*Beyond wavelets*’ (Academic Press, 2002, 1st edn.), pp. 1–30
- [25] Tang, L., Zhao, F., Zhao, Z.: ‘The nonsubsampled contourlet transform for image fusion’. Proc. Int. Conf. Wavelet Analysis and Pattern Recognition, Beijing, China, November 2007, pp. 305–310
- [26] Srivastava, R., Khare, A.: ‘Medical image fusion using local energy in nonsubsampled contourlet transform domain’. Proc. 5th Int. Conf. Computational Vision and Robotics, August 2014, pp. 29–35
- [27] Huimin, L., Yujie, L., Kitazono, Y., *et al.*: ‘Local energy based multi-focus image fusion on curvelet transform’. Proc. Int. Symp. on Communication and Information Technology (ISCT), October 2010, pp. 1154–1157
- [28] Yang, B., Li, S., Sun, F.: ‘Image fusion using nonsubsampled contourlet transform’. Proc. 4th Int. Conf. Image and Graphics, 2007, pp. 719–724
- [29] Li, S., Li, Z., Gong, J.: ‘Multivariate statistical analysis of measure for assessing the quality of image fusion’, *Int. J. Image Data Fusion*, 2010, **1**, (1), pp. 47–66
- [30] Shi, W., Zhu, C., Tian, Y., *et al.*: ‘Wavelet based image fusion and quality assessment’, *Int. J. Appl. Earth Obs. Geo Inf.*, 2005, **6**, (3), pp. 241–251
- [31] Tian, J., Chen, L., Ma, L., *et al.*: ‘Multi-focus image fusion using a bilateral gradient-based sharpness criterion’, *Opt. Commun.*, 2011, **284**, (1), pp. 80–87
- [32] Borwonwanadelok, P., Rattanapitak, W., Udomhunsakul, S.: ‘Multi-focus image fusion based on stationary wavelet transform and extended spatial frequency measurement’. Proc. Int. Conf. Electronic Computer Technology, Macau, China, February 2009, pp. 77–81
- [33] Deng, A., Wu, J., Yang, S.: ‘An image fusion algorithm based on discrete wavelet transform and Canny operator’. Int. Conf. Advance Research on Computer Education, Simulation and Modeling, Wuhan, China, June 2011, pp. 32–38
- [34] Lewis, J.J., O’Callaghan, R.J., Nikolov, S.G., *et al.*: ‘Pixel- and region-based image fusion with complex wavelets’, *Inf. Fusion*, 2007, **8**, (2), pp. 119–130
- [35] Xiaohong, X., Zhihong, W.: ‘Image fusion based on Lifting wavelet transform’. Proc. Int. Symp. on Intelligence Information Processing and Trusted Computing (IPTC), Huanggang, China, October 2010, pp. 659–662
- [36] Wang, H.: ‘A new multiwavelet-based approach to image fusion’, *J. Math. Imaging Vis.*, 2004, **21**, (2), pp. 177–192